Universiteit
Leiden
The Netherlands

Design, synthesis and application of sulfur-containing heterocycles for the inhibition of glycosidases and glycosyltransferases

Kok, K.

Citation
Kok, K. (2024, October 2). *Design, synthesis and application of sulfur-containing heterocycles for the inhibition of glycosidases and glycosyltransferases*. Retrieved from https://hdl.handle.net/1887/4093669

Version:	Publisher's Version
License:	Licence agreement concerning inclusion of doctoral thesis in the Institutional Repository of the University of Leiden
Downloaded from:	https://hdl.handle.net/1887/4093669

Note: To cite this publication please use the final published version (if applicable).

3

Trans-cyclosulfamidate mannose-configured cyclitol allows isoform-dependent inhibition of GH47 α-D-mannosidases through a bump-and-hole strategy

Manuscript published as:

Males, A.; Kok, K.; Nin-Hill, A.; de Koster, N.; van den Beukel, S.; Beenakker, T. J. M.; van der Marel, G. A.; Codée, J. D. C.; Aerts, J. M. F. G.; Overkleeft, H. S.; Rovira, C.; Davies, G. J.; Artola, M. Trans-cyclosulfamidate mannose-configured cyclitol allows isoform-dependent inhibition of GH47 α-D-mannosidases through a bump-and-hole strategy. *Chem. Sci.* **2023**, *14* (46), 13581–13586.

3.1 Introduction

Initially described by Koshland in 1953,[1] and with few exceptions, glycosidases follow two distinct reaction pathways leading to inversion or net retention of the configuration of the anomeric carbon after hydrolysis. Retaining enzymes (typically) harness a double-displacement mechanism via the formation and subsequent breakdown of a covalent intermediate flanked by an oxocarbenium-ion-like transition state, a mechanism which can be specifically hijacked using covalent inactivators.[2-4] In contrast, the one-step inverting mechanism involves an "S_N2" direct attack of water at the anomeric carbon through a single oxocarbenium ion transition-state rendering small molecule selective inhibition more challenging.[5] Regardless of the reaction mechanism, one serious challenge, addressed in this chapter for the inverting α-D-mannosidases, is the difficulty in specifically inhibiting single member of closely related enzyme families, whose active centers are identical, and for whom all members of the superfamily are inhibited similarly by small molecules.

Decades of work on diverse glycosidases (including α-D-mannosidases,[6-8] reviewed by Williams and collaborator [9,10]) has shown that the substrates undergo specific conformational fluctuations to accommodate their steric and electronic features. Indeed, conformational mimicry of the ligands along the reaction coordinates, Michaelis complex, transition state or product complexes, has been demonstrated to be of key relevance when designing inhibitors for specific carbohydrate hydrolases. GH47 mannosidases are Ca^{2+}-dependent metalloenzymes that follow a one-step inverting mechanism with a $^3S_1$ (Michaelis complex) → $^3H_4^{\ddagger}$ (transition state) → $^1C_4$ (product) conformational itinerary (Figure 3.1).[11,12]

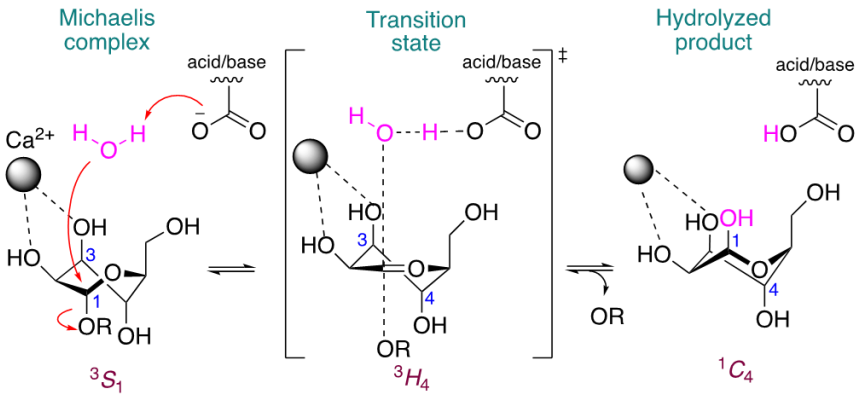

Figure 3.1. Conformational reaction itinerary of inverting GH47 α-D-mannosidases

Kifunensine **1** is one such conformationally restrained compound that achieves selective inhibition of the GH47 α-D-mannosidase family by virtue of mimicry of the mannose

configuration and $^{1}C_4$ conformation of the enzyme-product state (Figure 3.2).[13] Similarly, mannoimidazole **2** and 1-deoxymannojirimycin (DMJ) **3** also inhibit GH47 α-D-mannosidases, but do so by mimicking the oxocarbenium transition state ($^{3}H_4$) or both the Michaelis complex ($^{3}S_1$) and product ($^{1}C_4$) conformations, respectively (Figure 3.2). However, all are incapable of inhibiting individual GH47 α-D-mannosidases selectively which means they cannot be used for specific inhibition of single enzymes in cells.

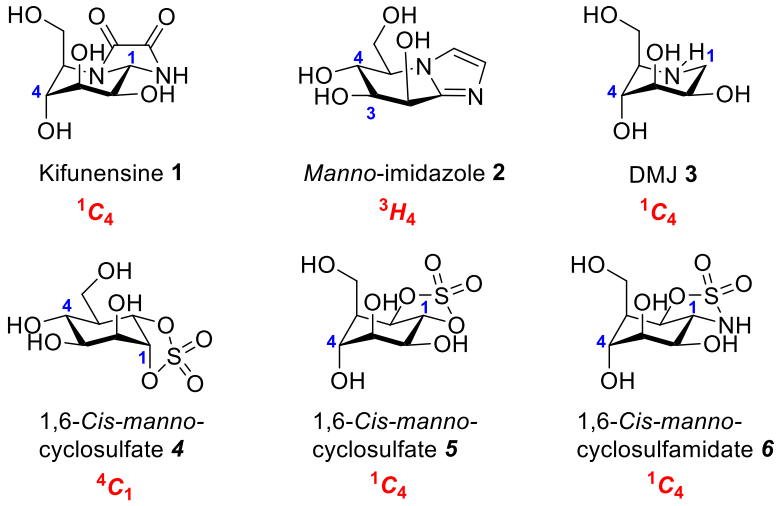

Figure 3.2. Chemical structures of known inhibitors Kifunensine **1**, mannoimidazole **2**, 1-deoxymannojirimycin (DMJ) **3** and new molecules developed in this work 1,6-*cis*-manno-cyclosulfate **4**, 1,6-*trans*-manno-cyclosulfate **5** and 1,6-*trans*-manno-cyclosulfamidate **6**.

GH47 Class I inverting α-D-mannosidases hydrolyse 1,2-mannosidic linkages and are responsible for the processing of N-glycans, ultimately regulating the maturation and quality control of glycoproteins in the secretory pathway.[14] GH47 mannosidases can be divided into three subfamilies within the endoplasmic reticulum (ER) and Golgi apparatus. The cleavage of α-1,2-mannoside linkages in $Man_9GlcNAc_2$-Asn substrates is initiated by ERMI (first subfamily) followed by Golgi-α-1,2-mannosidases, GMIA, GMIB, GMIC (second subfamily), hydrolysing subsequent α-1,2-mannoside branches and affording $Man_5GlcNAc_2$-Asn (Figure 3.3). The third subfamily comprises of ER degradation enhancing α-mannosidase-like (EDEM) enzymes (EDEM1, EDEM2 and EDEM3) that target misfolded proteins and mark them for degradation via ER-associated degradation (ERAD) machinery.

Given the success of generic conformational mimicry for enzymes of this family [12,13,15] (notwithstanding the fact that humans have a large multigene family of GH47 enzymes), it was envisioned that cyclic sulfates and sulfamidates might possess similar conformational attributes.

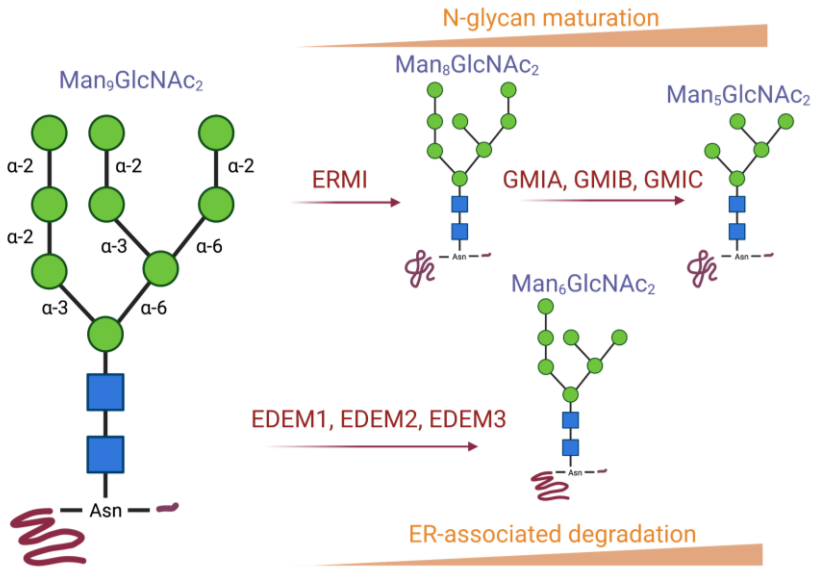

Figure 3.3. GH47 Class I inverting α-D-mannosidase: α-1,2-mannosidases, ERMI, GMIA, GMIB, GMIC, are involved in N-glycan maturation whereas EDEM1, EDEM2 and EDEM3 play a key role in the ER-associated degradation (ERAD) machinery.

Recently, it has been demonstrated that a cyclophellitol analogue bearing a *cis*-cyclic sulfate electrophile is a selective nanomolar covalent α-glucosidase inhibitor by virtue of its $^{4}C_{1}$ Michaelis complex mimicry.[2] Substitution of this cyclic sulfate by an unreactive 1,6-cyclosulfamidate yielded diverse α-glucosidase[16] and α-galactosidase[17] competitive inhibitors with great potential as enzyme stabilizers for the treatment of lysosomal storage disorders such as Pompe or Fabry disease. Building upon the capability of *cis*-cyclic sulfates and sulfamidates to lock their compounds in a $^{4}C_{1}$ chair conformation[2,16-18] it was hypothesized that *trans*-cyclic sulfate **5** and sulfamidate **6** may instead invert this chair, yielding a new class of $^{1}C_{4}$ locked conformational glycosidase inhibitors (Figure 3.2).

This chapter describes the design and synthesis of an α-D-mannose configured 1,6-*trans*-cyclic sulfamidate as a potential inhibitor of the GH47 α-D-mannosidase family. QM calculations of free energy landscapes, illustrates that cyclosulfamidate **6** favours a $^{1}C_{4}$ chair conformation consistent with the GH47 conformational itinerary. A steric clash in the enzyme active centre enables the implementation of a bump-and-hole methodology for GH47 inhibition. Mutation of a leucine, conserved across the GH47 α-D-mannosidase family, to serine unlocks the dormant inhibition of **6** leading to a 570 nM inhibitor specific for the mutant enzyme only. This chapter integrates conformational mimicry and bump-and-hole strategies to enable the specific inhibition of individual, but closely related, α-D-mannosidase within the GH47 family.

3.2 Results and discussion

3.2.1 *In silico* conformational analysis

The intrinsic conformational preference of mannose-configured cyclic sulfates and sulfamidate **4**-**6** was analysed employing QM metadynamics simulations to reconstruct a free energy landscape (FEL). The FELs show that opposite to the $^4C_1$ conformation adopted by 1,6-*cis*-cyclic sulfate **4** (Figure 3.4A), both *trans*- **5** and **6** have a strong conformational preference for a flipped $^1C_4$ (Figure 3.4B and 3.4C). The sugar ring of **4** is quite flexible, but the relaxed chair conformation ($^4C_1$) is the most stable, followed by $B_{2,5}$ and $^1C_4$, which are ≈ 3 kcal·mol^{-1} higher in energy. On the contrary, the FELs of **5** and **6** show that the 1,6-*trans* compounds are highly confined in the southern hemisphere. Both $^1S_3$ and $^1C_4$ conformations are thermally accessible, but $^1C_4$ is the most stable. Given the preference for this conformation, the *manno*-configured 1,6-*trans*-cyclic sulfate **5** and/or sulfamidate **6** were synthesized in order to establish whether, similar to kifunensine, compounds **5** and/or **6** would act as a GH47 α-D-mannosidase inhibitor.

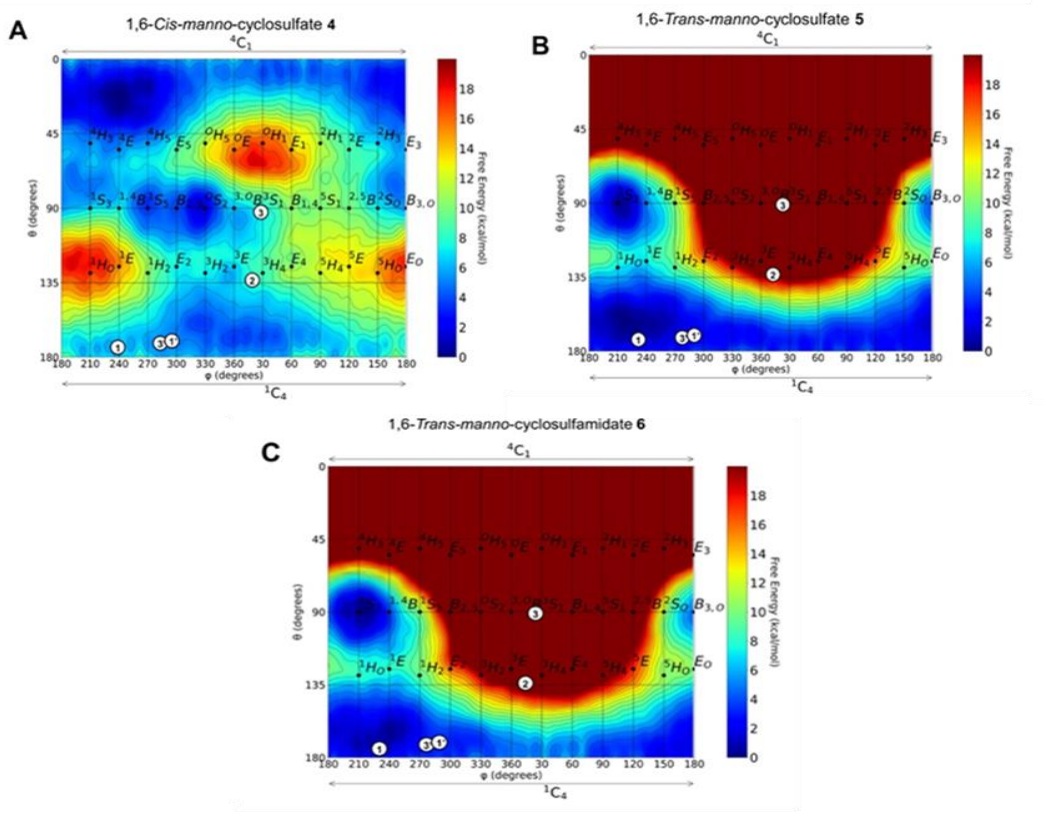

Figure 3.4. Conformational free energy landscapes (FELs, Mercator projection) contoured at 1 kcal·mol^{-1} of A) 1,6-*cis*-manno-cyclosulfate **4**, B) 1,6-*trans*-manno-cyclosulfate **5** and C) 1,6-*trans*-manno-cyclosulfamidate **6**.

3.2.2 Design and synthesis of GH47 inverting α-D-mannosidase inhibitors

1,6-*Cis*-manno-cyclosulfate **4**, 1,6-*trans*-manno-cyclosulfate **5** and 1,6-*trans*-manno-cyclosulfamidate **6** were synthesized from mannose-configured tetra-*O*-benzyl-cyclohexene **7**, respectively. For the synthesis of *cis*-cyclosulfate **4** (Scheme 3.1), cyclohexene **7** was dihydroxylated by *in situ* formation of RuO_4 as the oxidizing agent. The obtained diol **8** was converted to an intermediate cyclic sulfite by reaction with $SOCl_2$ under basic conditions. Subsequent oxidation resulted in the formation of cyclic sulfate **9**. Deprotection of **9** resulted initially in the partial formation of **4**. However, the resulting product quickly degraded towards epoxide **10** though opening of the cyclic sulfate by the 2-OH pseudo anomeric hydroxyl. It's *trans*-configured analogue **5** was synthesized in a similar fashion from *trans*-diol **12**, which was obtained through the nucleophilic opening of epoxide **11** under acidic conditions. Similar to compound **4**, and although *trans*-cyclosulfate **5** could be isolated and purified, it degraded over time at -20 °C.

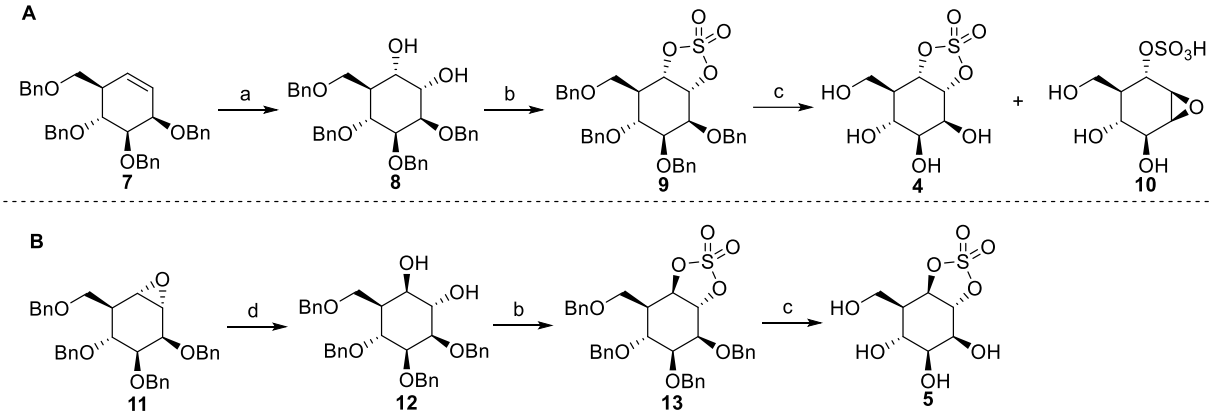

Scheme 3.1. Synthesis of *cis*-cyclosulfate **4** (A) and *trans*-cyclosulfate **5** (B)**.** Reagents and conditions: (a) $RuCl_3{\cdot}H_2O$, $NaIO_4$, ACN, EtOAc, H_2O, 78%; (b) (i) $SOCl_2$,Et_3N, imidazole, DCM, 0 ℃; (ii) $RuCl_3{\cdot}H_2O$, $NaIO_4$, ACN, EtOAc, H_2O, 41% (**9**), 78% (**13**); (c) Pd/C, H_2, MeOH, 50% (**10**), 75% (**5**); (d) H_2SO_4, H_2O, THF, 80 ℃, 81%.

The synthesis of the potentially more stable cyclosulfamidate **6** (Scheme 3.2) started with the addition of sodium azide to tetra-*O*-benzyl-cyclophellitol **7** which resulted in a mixture of diastereomers **15** and **16**. Azide **16** was subsequently reduced using PtO_2 to obtain amine **17**. Cbz-protection of the amine gave intermediate **18** which was treated with $SOCl_2$ followed by $RuCl_3/NaIO_4$-mediated oxidation of the formed sulfites, resulting in the formation of fully protected *trans*-sulfamidate **19**. *Trans*-sulfamidate **19** was then exposed to hydrogenation conditions to obtain cyclosulfamidate **6** which proved to be chemically stable.

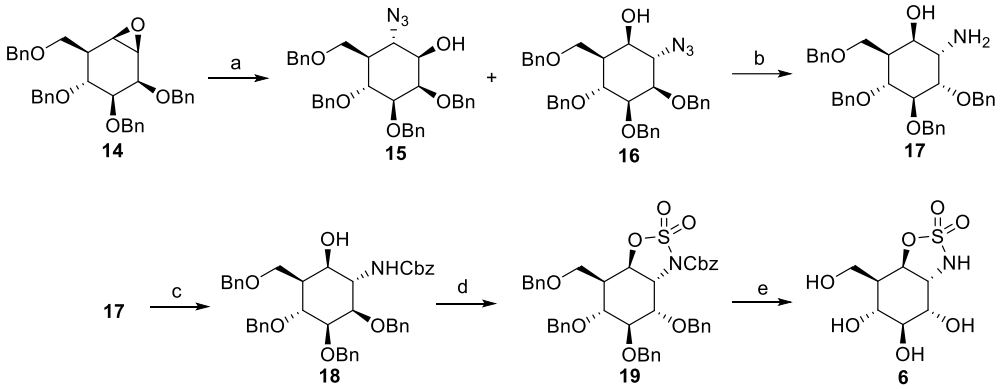

Scheme 3.2. Synthesis of 1,6-*trans*-manno-cyclosulfamidate **6**. Reagents and conditions: (a) NaN_3, $LiClO_4$, DMF, 100 °C, 58% (**15**) and 14% (**16**); (b) PtO_2, H_2, THF, rt, 86%; (c) benzyl chloroformate, K_2CO_3, dioxane, H_2O, rt, 74%; (c) (i) $SOCl_2$, Et_3N, imidazole, DCM, 0 °C; (ii) $RuCl_3{\cdot}H_2O$, $NaIO_4$, ACN, EtOAc, H_2O, 46%; (d) Pd/C, H_2, MeOH, 75%.

3.2.3 *In vitro* evaluation of *trans*-mannose-cyclosulfamidate inhibitor

Surprisingly, no significant inhibition of the GH47 model enzyme (whose active center is identical to the human enzymes) from *Caulobacter* K31 strain was observed even at high inhibitor concentrations; 82% of α-1,2-mannobiose was hydrolysed by the WT GH47 mannosidase to mannose after the addition of 1 mM of **6** (Figure S3.1) in contrast to kifunensine (K_D of 39 nM),[13] mannoimidazole (K_D of 47 nM),[12] and DMJ (K_D of 481 nM)[15]). Accordingly, crystal soaks revealed no binding. Simple overlay of **6** over published complexes of the *Caulobacter* GH47 enzyme revealed a likely steric clash between one of the oxygen atoms of the sulfamidate group of **6** with the Cδ2 atom of a leucine side chain, conserved across the GH47 family, in the active centre of the enzyme (Figure 3.5).

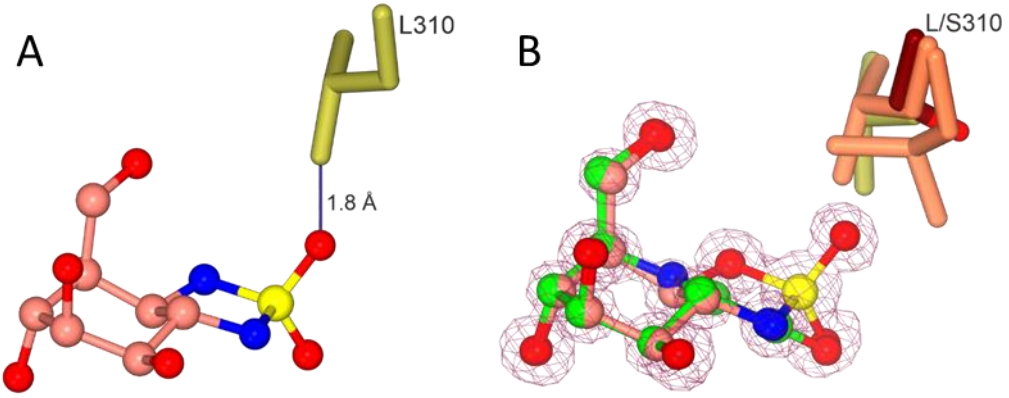

Figure 3.5. Docking of **6**, in pink, into the crystal structure of *Caulobacter* GH47 (PDB ID: 4AYO), in gold, showing the distance between the oxygen of **6** and L310. A: **6** was docked into the *Ck*GH47 enzyme active site by least squares fit superposition in coot against the *Ck*GH47 and kifunensine complex (PDB ID 5NE5). B: Position of *Ck*GH47 WT crystal structures of the inhibitors **6** (pink) and kifunensine (green); native is shown in gold (PDB ID: 4AYO) and *Ck*GH47 in complex with kifunensine is shown in orange (PDB ID: 5NE5).

Although this initial observation was fortuitous, it immediately presented a solution to the specific inhibition of individual enzymes problem. In contrast to other known GH47 inhibitors, the leucine clash could be exploited to formulate a "bump-and-hole" strategy enabling selective individual α-mannosidase GH47 inhibition, otherwise not possible through chemical knockdown. Originally developed for kinases by Shokat[20,21] and recently also deployed in the glycoscience context by Schumann,[21,22] bump-and-hole engineering is best applied to large multigene families where allele-specific inhibition is challenging. This strategy relies on introducing a "bump" on the inhibitor/ligand/substrate that is accommodated specifically by enzyme variants into which a complementary "hole" has been created through mutagenesis. Since, despite conformational matching, **6** failed because of encountering a "bump", it was hypothesized that exchanging the leucine for a smaller amino-acid would form an appropriate "hole" to accommodate **6** in a variant-specific manner. As proof-of-concept, mutation to a serine was selected because of the potential to form a hydrogen bond to the inhibitor in addition to removing the steric clashing distance: a hole with benefits. The L310S variant was created and shown to be catalytically viable in the degradation of α-1,2-mannobiose (Figure 3.6A, 3.6B and Table S3.1**)**. The V_{max} value of 0.15 μM s^{-1} and the K_M value of 403 μM for the mutant was 10x and 6x lower than the WT.[23,24] Similar loss in enzyme catalytic activity has also been observed in protein kinase bump and hole approaches.[19,20]

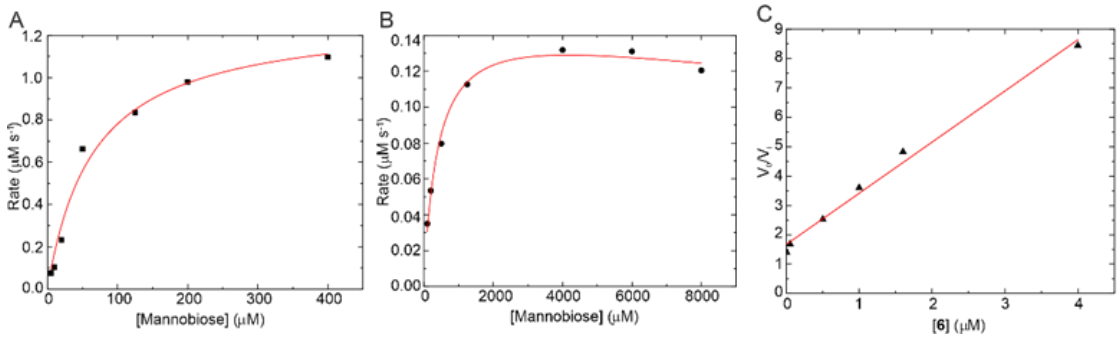

Figure 3.6. Catalytic activity of *Ck*GH47 WT compared to *Ck*GH47 L310S mutant. A) *Ck*GH47 Michaelis-Menten kinetics (fitting model) over a range of α-1,2-mannobiose concentrations. B) *Ck*GH47 L310S Michaelis-Menten kinetics over a range of α-1,2-mannobiose concentrations fitted to a substrate inhibition model. C) The K_i, derived from the gradient ($1/K_i$), for **6** against *Ck*GH47 L310S.

Building on this kinetic assay, an inhibition constant was obtained by pre-incubation of the enzyme and **6** for 30 minutes and then following the same time-point procedure as for the Michaelis-Menten assay. Thus following the approach described by Suits *et al.*[25], a 574 nM K_i was obtained for **6** with the L310S mutant specifically (Figure 3.6C, Table S3.1). Similarly, a dissociation constant of 970 nM was obtained using isothermal titration calorimetry (Figure

S2). To understand the interactions between **6** and *Ck*GH47 L310S regarding the introduced hole, a crystal structure complex was obtained (statistics in Table S2). *Trans*-cyclicsulfamidate **6** binds similarly to other conformationally-restricted GH47 inhibitors, with additional interactions between the sulfamidate and active site residues, for example, the nitrogen and oxygen, and D249 and R363 side chains. Additionally, the introduced serine residue is indeed now in a position to form a hydrogen bond to the oxygen of the sulfamidate with a distance of 3.1 Å. Also validating the initial design hypothesis, overlaying the L310S structure with **6** with that of the WT *Ck*GH47 native enzyme revealed 1.3-1.9 Å steric clashes of **6** to Leucine 310 (Figure 3.5).

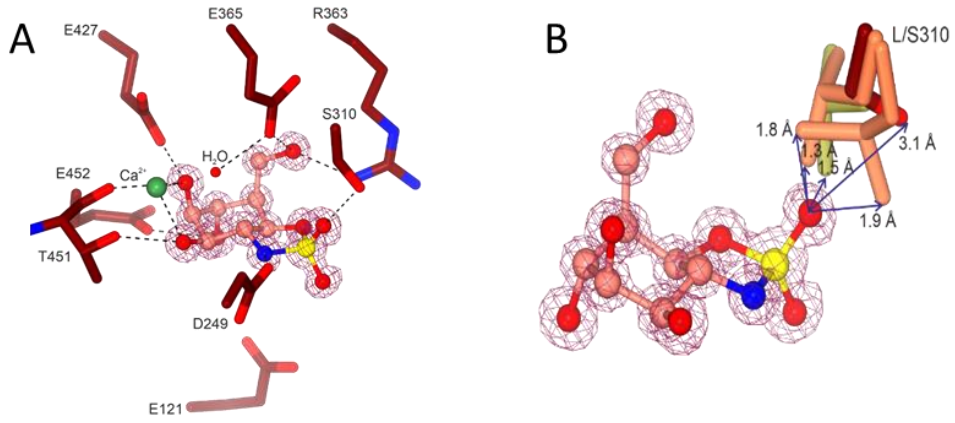

Figure 3.5. Structure of *Ck*GH47 L310S in complex with **6**. A) Active site residues (dark red) within hydrogen bonding distance to **6** (pink) in the -1 subsite. The maximum-likelihood/σ_A-weighted $2F_{obs} - F_{calc}$ map, shown in purple, is contoured at 1.3 e Å^{-3}. B) Superposition of *Ck*GH47 WT crystal structures highlighting the flexibility of residue 310; native is shown in gold (PDB ID: 4AYO) and *Ck*GH47 in complex with kifunensine is shown in orange (PDB ID: 5NE5).

3.3 Conclusion

"Allele-specific" inhibition of single members of multigene families is a major challenge in chemical glycobiology. This chapter illustrate the dual approach of conformational mimicry with bump and hole to establish nanomolar inhibitor-enzyme pair: 1,6-*trans*-cyclic sulfamidate **6** and a L310S variant that allows selective inhibition of a α-1,2-mannosidase. Importantly, the leucine residue is conserved across all seven human ER and Golgi α-1,2-mannosidases (Figure S3.3). In summary, this work lays the foundation for targeted enzyme inactivation campaigns for α-1,2-mannosidases to understand the roles of the different inverting GH47 α-1,2-mannosidases in cellular biology and disease.[26-28]

3.4 Acknowledgements

Dr. Alexandra Males, Prof. Dr. Gideon J. Davies and Nicky de Koster are kindly acknowledged for the inhibition kinetics, selectivity assays and crystallographic studies described in this chapter and their valuable discussions. Similarly, Alba Nin-Hill and Prof. Dr. Carme Rovira are kindly acknowledged for providing the conformational free energy landscapes and their valuable discussion. Finally, I want to acknowledge Thomas J.M. Beenakker and Sija van den Beukel for their contribution to the synthesis of the compounds in this chapter.

3.5 Experimental methods

3.5.1 Biochemical and biological methods

3.5.1.1 *Ck*GH47 WT and L310S mutant inhibition and kinetics assays

For all assays, *Ck*GH47 WT enzyme was diluted to 200 nM, and *Ck*GH47 L310S was diluted to 500 nM into buffer containing 50 mM HEPES pH 7.0, 100 mM NaCl and 2 mM $CaCl_2$. To obtain Michaelis-Menten kinetics for the wildtype enzyme, a range of α-1,2-mannobiose substrate concentrations from 5 to 400 μM and time points of 1, 2, 3, 4, 5 minutes were used. To obtain Michaelis-Menten kinetics for the L310S mutant enzyme, a range of α-1,2-mannobiose substrate concentrations from 100 μM to 8 mM and time points of 5, 10, 15, 20 minutes were used. Lastly, to achieve an inhibition constant, the method described by Suits and colleagues was used whereby the substrate α-1,2-mannobiose concentration (130 μM) was greatly less than the K_M ([S]<<K_M).[6] The gradient of the graph, V_0/V_i (absence and presence of inhibitor) against a range of **6** inhibitor concentrations from 5 nM to 4 μM, was $1/K_i$. Time points were taken at 5, 10, 20 and 30 minutes. After taking each time point, the sample was heat denatured at 95 °C for 5 minutes. The reactions were conducted in triplicate and averaged.

The samples were plated into a 384-well clear plate and absorbance was monitored using an Epoch microplate spectrophotometer (BioTek). The mannose detection kit (Megazyme) was used to detect the presence of mannose through a coupled assay whereby the final step, the formation of NADPH and gluconate-6-phosphate from $NADP^+$ and glucose-6-phosphate by glucose-6-phosphate dehydrogenase, was monitored at 340 nm. The absorbance after hexokinase was added to the mixture (phosphorylation of mannose producing mannose-6-phosphate) was subtracted from the final absorbance. A standard curve of absorbance against a range of mannose concentrations was used to determine the concentration of mannose produced in the enzyme reactions.

3.5.1.2 Isothermal titration calorimetry

*Ck*GH47 L310S and **6** were diluted into buffer containing 50 mM HEPES pH 7.0, 100 mM NaCl and 2 mM $CaCl_2$. 300 μM **6** was added by syringe to 20.4 μM *Ck*GH47 L310S in the calorimeter cell using a MicroCal ITC200 calorimeter at 25 °C over 20 injections. The experiment was duplicated to obtain a consistent K_D value. The binding affinity was obtained using the one set of sites fitting model within the MicroCal PEAK-ITC analysis software.

3.5.2 Crystallographic data collection and refinement of *Ck*GH47

*Ck*GH47 WT gene cloned into the pET21a vector was mutated using the Q5 site-directed mutagenesis kit (New England Biolabs) where the forward primer was 5′-ACAGAGCGAAtcgGCCGCATATTATGCGGG-3′ and the reverse primer was 5′-GCGGTACCGGTAACCGCA-3′. Protein production and purification was followed as described previously.[3] Using the hanging drop method, 12.5 mg mL^{-1} *Ck*GH47 L310S protein crystallised under the conditions 23% PEG3350, 0.1 M MES pH 7.0, 0.2 M ammonium acetate. A 20-times diluted seed stock of *Ck*GH47 WT crystals was used to aid crystallisation; the protein to reservoir to seed stock ratio was 0.5:0.4:0.1. Mature crystals were soaked with 2.5 mM **6** for 72 hrs. Structure data were collected on the Diamond I03 MX beamline. Reference data in the form of a reflections file and a Free R flag data set were copied from PDB ID: 4AYO and used in indexing and integration using AIMLESS from the CCP4i2 software suite.[3][7] Refinement of the model was conducted through cycles of REFMAC and manual model building in COOT.[8][9] Validation of the ligand conformation was conducted using PRIVATEER. Details of the data collection and refinement statistics are shown in Table **S2**. Figures of the structure were produced by using CCP4mg.

3.5.3 Chemical synthesis

3.5.3.1 General experimental details

All reagents were of experimental grade and were used without further purification unless stated otherwise. Dichloromethane (DCM) and tetrahydrofuran (THF) were stored over 3 Å molecular sieves and *N,N*-dimethylformamide (DMF) was stored over 4 Å molecular sieves, which were dried *in vacuo* before use. All reactions were performed under an N_2 atmosphere unless stated otherwise. Reactions were monitored by analytical thin layer chromatography (TLC) using Merck aluminum sheets pre-coated with silica gel 60 with detection by UV-absorption (254 nm) and by spraying with a solution of $(NH_4)_6Mo_7O_{24}\cdot H_2O$ (25 g/L) and $(NH_4)_4Ce(SO_4)_4\cdot H_2O$ (10 g/mL) in 10% sulfuric acid followed by charring at ~150 ℃ or by spraying with an aqueous solution of $KMnO_4$ (7%) and K_2CO_3 (2%) followed by charring at ~150 ℃. Column chromatography was performed manually using either Baker or Screening Device silica gel 60 (0.04-0.063 mm) or a Biotage Isolera™ flash purification system using silica gel cartridges (Screening Device SilicaSep HP, particle size 15-40 μm, 60A) in the indicated solvents. ^{1}H-NMR and ^{13}C-NMR spectra were recorded on Bruker AV-500 (500/126 MHz), and Bruker AV-400 (400/101 MHz) spectrometer in the given solvent. Chemical shifts are given in ppm (δ) relative to the chloroform, methanol or dimethylsulfoxide residual solvent peak or tetramethylsilane (TMS) as internal standard. All given ^{13}C-NMR spectra are proton decoupled. The following abbreviations are used to describe peak patterns when appropriate: s (singlet), d (doublet), t (triplet), q (quartet), m (multiplet), Ar (aromatic), C_q (quarternary carbon). 2D NMR experiments (HSQC, COSY) were carried out to assign protons and carbons of the new structures and numbering and assignation follows the general numbering shown in compound **8** (See synthesis and characterization section). High-resolution mass spectra (HRMS) of compounds were recorded with an LTQ Orbitrap (Thermo Finnigan) equipped with an electronspray ion source in positive mode (source voltage 3.5 kV, sheath gas flow 10 mL/min, capillary temperature 250 ℃) with resolution R = 60000 at m/z (400 mass range m/z = 150 – 2000) and dioctyl phthalate (m/z = 391.28428) as a lock mass. The high-resolution mass spectrometer was calibrated prior to measurements with a calibration mixture (Thermo Finnigan). Optical rotations were measured on a Anton Paar MCP automatic polarimeter (Sodium D-line, λ = 589 nm). LC-MS analysis was performed on a LCQ Advantage Max (Thermo Finnigan) ion-trap spectrometer (ESI+) coupled to a Surveyor HPLC system (Thermo Finnigan) equipped with a C18 column (Gemini, 4.6 mm x 50 mm, 3 μM particle size, Phenomenex) equipped with buffers A: H_2O, B: acetonitrile (MeCN) or an Agilent technologies 1260 infinity LC-MS with a 6120 Quadrupole MS system equipped with buffers A: H_2O, B: acetonitrile (MeCN) and C: 100 mM NH_4OAc. IR spectra were recorded on a Shimadzu FTIR-8300 and are reported in cm^{-1}.

3.5.3.2 Synthesis and characterization

(1*S*,2*S*,3*R*,4*S*,5*R*,6*S*)-3,4,5-Tris(benzyloxy)-6-((benzyloxy)methyl)cyclohexane-1,2-diol (8): To a solution of

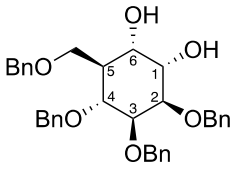

mannose configured perbenzylated cyclohexene **7** (1.04 g, 2.0 mmol) in EtOAc/ACN (1:1, 60 mL), a solution of sodium periodate (0.64 g, 3.0 mmol, 1.5 eq.) and catalytic amount of ruthenium(III) chloride trihydrate (36 mg, 0.14 mmol, 0.07 eq.) in H_2O (16 mL) was added at 0 °C. After vigorously stirring for 1 h, the reaction mixture was quenched with 10% aqueous $Na_2S_2O_3$ (15 mL) and diluted with sat. aq. $NaHCO_3$ solution and EtOAc. The aqueous phase was separated and extracted with EtOAc (3x) and the combined organic layers were washed with brine, dried over $MgSO_4$ and concentrated *in vacuo*. Purification by column chromatography (Pentane/EtOAc from 7:3 to 6:4 gave exclusively α-diol **8** (0.746 g, 1.34 mmol, 68%) as a clear oil. ^{1}H NMR (400 MHz, $CDCl_3$): δ 7.40 – 7.24 (m, 18H, CH_{Ar}), 7.22 – 7.17 (m, 2H, CH_{Ar}), 4.89 (d, J = 11.0 Hz, 1H, CH*H*Ph), 4.78 (d, J = 12.2 Hz, 1H, CH*H*Ph), 4.69 – 4.59 (m, 3H, CH*H*Ph), 4.49 (s, 2H, CH*H*Ph), 4.45 (d, J = 10.9 Hz, 1H, CH*H*Ph), 4.06 – 3.91 (m, 5H, H-1, H-2, H-3, H-7A, H-7B), 3.64 (t, J = 9.3 Hz, 1H, H-6), 3.56 (t, J = 9.0 Hz, 1H, H-4), 2.60 (s, 1H, OH), 2.23 (qd, J = 9.4, 3.3 Hz, 1H, H-5). ^{13}C NMR (101 MHz, $CDCl_3$) δ 138.7, 138.5, 138.5, 137.4 (C_{qAr}), 128.6, 128.4, 128.1, 128.0, 127.8, 127.7, 127.6 (CH_{Ar}), 81.2 (C-1/C-2/C-3), 75.9 (C-6), 75.7 (C-1/C-2/C-3), 75.0 (C-1/C-2/C-3), 73.6, 73.3, 72.6, (CH_2Ph), 71.8 (C-4), 71.8 (C-7), 70.0 (C-1/C-2/C-3), 42.7 (C-5). HRMS: calculated for $[C_{35}H_{38}O_6]^+$ 555.27412, found 555.27433.

(3a*R*,4*S*,5*S*,6*R*,7*R*,7a*S*)-4,5,6-Tris(benzyloxy)-7-((benzyloxy)methyl)hexahydrobenzo[*d*][1,3,2] dioxathiole 2,2-dioxide (9): Diol **8** (0.36 g, 0.65 mmol) was dissolved in DCM (30 mL) and Et_3N (0.33 mL, 2.4 mmol, 3.7

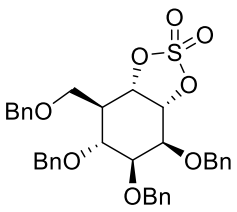

eq.) was added at 0 °C. Next, thionyl chloride (0.15 mL, 2.1 mmol, 3.2 eq.) was slowly added over 5 min. After stirring for 1 h, additional Et_3N (90 µL, 0.65 mmol, 1 eq.) and thionyl chloride (45 µL, 0.65 mmol, 1 eq.) was added. The reaction mixture was stirred for an additional 30 min before quenching with cold H_2O and dilution with cold Et_2O. The layers were separated and the organic layer was washed with H_2O (2x), dried over $MgSO_4$, filtered and concentrated *in vacuo*. Purification by column chromatography (3.5% EtOAc in pentane) gave the sulfite diastereomeric mixture (390 mg) as an orange oil. HRMS: calculated for $[C_{35}H_{37}O_7S]^+$ 601.22545, found 601.22584. Afterwards, to a solution of the sulfite diastereomeric mixture (192 mg, 0.32 mmol) in CCl_4/MeCN (1:1, 24 mL) was added a solution of sodium periodate (0.137 g, 0.64 mmol, 2.0 eq.) and a catalytic amount of ruthenium(III) chloride trihydrate (6 mg, 22 µmol, 0.07 eq.) in H_2O (12 mL) at 0 °C. After vigorously stirring for 1.5 h, the reaction mixture was diluted with Et_2O and H_2O. The organic layer was separated, washed with brine, dried over $MgSO_4$ and concentrated *in vacuo*. Purification by column chromatography (8% EtOAc in pentane) gave title compound **9** (81 mg, 0.131 mmol, 41% over 2 steps) as a white solid. ^{1}H NMR (400 MHz, $CDCl_3$) δ 7.40 – 7.20 (m, 18H, CH_{Ar}), 7.14 (dd, J = 7.3, 2.2 Hz, 2H, CH_{Ar}), 5.29 (dd, J = 11.2, 6.4 Hz, 1H, H-6), 5.20 (t, J = 6.2 Hz, 1H, H-1), 4.73 (dd, J = 19.8, 11.8 Hz, 1H, CH*H*Ph), 4.59 (d, J = 4.2 Hz, 2H, CH*H*Ph), 4.59 – 4.51 (m, 1H, CH*H*Ph), 4.43 (d, J = 11.7 Hz, 2H, CH*H*Ph), 4.31 (d, J = 11.9 Hz, 1H, CH*H*Ph), 4.22 (d, J = 11.5 Hz, 1H, CH*H*Ph), 4.11 (d, J = 1.6 Hz, 1H, H-2), 3.82 – 3.78 (m, 2H, H-3, H-4), 3.58 (dd, J = 9.6, 2.8 Hz, 1H, H-7B), 3.52 (dd, J = 9.6, 2.7 Hz, 1H, H-7A), 2.21 (ddt, J = 11.1, 8.2, 2.8 Hz, 1H, H-5) ^{13}C NMR (101 MHz, $CDCl_3$) δ 138.0, 137.6, 137.5, 137.4 (C_{qAr}), 128.7, 128.6, 128.5, 128.2, 128.1, 128.0, 127.9, 127.7 (CH_{Ar}), 83.6 (C-1) , 80.0 (C-6), 76.5 (C-2), 76.2 (C-3), 74.2 (C-4), 73.2, 72.9, 72.8, 72.6 (CH_2Ph), 64.8 (C-7), 42.5 (C-5). HRMS: calculated for $[C_{35}H_{36}O_8SNa]^+$ 639.20231, found 639.20238.

(3a*R*,4*S*,5*S*,6*R*,7*R*,7*aS*)-4,5,6-Trihydroxy-7-(hydroxymethyl)hexahydrobenzo[*d*][1,3,2] dioxathiole 2,2-dioxide (10): Benzylated sulfate **9** (70 mg, 0.11 mmol) was dissolved in MeOH (10 mL). The reaction mixture

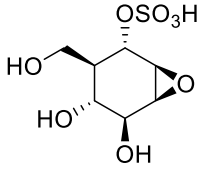

was purged with nitrogen gas and 10% palladium on carbon (15 mg) was added. Afterwards, the reaction vessel was purged with hydrogen and vigorously stirred overnight. The palladium catalyst was then filtered off followed by concentration *in vacuo*. Purification by column chromatography (10% MeOH in DCM → 20% MeOH in DCM) yielded compound **10** (14 mg, 55 µmol, 50 %) as a clear oil. ^{1}H NMR (500 MHz, MeOD) δ 4.20 (d, J = 2.0 Hz, 1H, H-1), 4.15 (d, J = 5.2 Hz, 1H, H-6), 4.08 (d, J = 5.3 Hz, 1H, H-4), 4.04 – 3.97 (m, 1H, H-2), 3.79 – 3.73 (m, 1H, H-3), 3.59 (dd, J = 10.6, 6.3 Hz, 1H, H-7B), 3.51 – 3.43 (m, 1H, H-7A), 2.25 – 2.20 (m,

1H, H-5). ^{13}C NMR (126 MHz, MeOD) δ 88.3 (C-1), 83.2 (C-6), 82.6 (C-3), 76.2 (C-2), 74.3 (C-4), 64.1 (C-7), 45.7 (C-5). HRMS: not found.

(1*R*,2*S*,3*R*,4*S*,5*R*,6*S*)-3,4,5-Tris(benzyloxy)-6-((benzyloxy)methyl)cyclohexane-1,2-diol (12): Fully benzylated β-mannose-configured cyclophellitol **11** (1.00 g, 1.86 mmol) was dissolved in THF (10 mL) and 3 M aq. H_2SO_4 (20 mL) was added and the resultant mixture was stirred at 80 ºC for 18 h. By TLC one main new spot can be observed. The reaction mixture was then allowed to cool to rt and the residue was dissolved in Et_2O (50 mL) and quenched with $NaHCO_3$ and extracted with Et_2O. The combined organic layers were dried over $MgSO_4$ and concentrated in *vacuo*. Purification by silica gel column chromatography (pentane /EtOAc 70:30 → 60:40) yielded **12** (0.84 g, 1.51 mmol, 81%). ^{1}H NMR (400 MHz, $CDCl_3$) δ 7.35 – 7.17 (m, 20H, CH_{Ar}), 4.63 – 4.37 (m, 8H, CH*H*Ph), 4.03 – 3.94 (m, 2H, H-1, H-6), 3.92 – 3.79 (m, 3H, H-3, H-4, H-7B), 3.74 – 3.66 (m, 2H, H-2, H-7B), 3.45 (s, 1H, OH), 2.85 (s, 1H, OH), 2.62 (q, J = 6.7, 5.9 Hz, 1H, H-5). ^{13}C NMR (101 MHz, $CDCl_3$) δ 138.3, 138.2, 138.1 (C_{qAr}), 128.5, 128.4, 128.4, 128.4, 128.0, 127.9, 127.9, 127.8, 127.7, 127.7 (CH_{Ar}), 79.8 (C-2), 74.8 (C-3/4), 73.2, 72.9, 72.8 (CH_2Ph), 71.6 (C-1), 70.7 (C-6), 67.9 (C-7), 42.7 (C-5). HRMS: calculated for $[C_{35}H_{38}O_6]^+$ 555.27412, found 555.27429.

(3*aR*,4*S*,5*S*,6*R*,7*R*,7*aR*)-4,5,6-Tris(benzyloxy)-7-((benzyloxy)methyl)hexahydrobenzo[*d*][1,3,2] dioxathiole 2,2-dioxide (13): To a solution of the diol **12** (96 mg, 0.17 mmol), Et_3N (0.12 mL, 0.87 mmol, 5 eq) and imidazole (59 mg, 0.87 mmol, 5 eq) in DCM (10 mL) at 0 ºC was added $SOCl_2$ (0.11 mL, 1.56 mmol) over 5 min and stirred for 2 h. The reaction mixture was diluted with cold Et_2O (20 mL) and washed with cold water (2 x 20 mL) and brine (30 mL). The organic layer was dried over $MgSO_4$ and filtered. The filtrate was concentrated and the residual triethylamine was removed under high vacuum (ca. 1 h). The resulting oil was dissolved in MeCN (4 mL) and CCl_4 (4 mL), and the solution cooled in an ice-bath. A solution of catalytic amount of $RuCl_3 \cdot 3H_2O$ and $NaIO_4$, (74 mg, 0.35 mmol) in H_2O was added and the reaction was stirred at rt overnight. EA (20 mL) and H2O (20 mL) were added and the two layers were separated. The aqueous layer was extracted with Et_2O (2 x25 mL) and the combined organic extracts were washed with brine (2 x 25 mL), dried over $MgSO_4$ filtered and concentrated *in vacuo*. Purification by column chromatography (8% EtOAc in pentane) gave title compound **13** (83 mg, 0.13 mmol, 78% over 2 steps). ^{1}H NMR (400 MHz, $CDCl_3$) δ 7.38 – 7.22 (m, 17H, CH_{Ar}), 7.16 (ddd, J = 11.1, 6.6, 2.1 Hz, 3H, CH_{Ar}), 5.18 (t, J = 10.4 Hz, 1H, H-1), 5.00 (dd, J = 10.8, 5.9 Hz, 1H, H-6), 4.72 (d, J = 11.8 Hz, 1H, CH*H*Ph), 4.58 (d, J = 11.9 Hz, 1H, CH*H*Ph), 4.55 – 4.35 (m, 5H, 5x CH*H*Ph), 4.38 – 4.28 (m, 1H, CH*H*Ph), 4.11 (t, J = 2.7 Hz, 1H, H-4), 4.02 (dd, J = 10.0, 3.3 Hz, 1H, H-2), 3.89 (t, J = 3.3 Hz, 1H, H-3), 3.82 (t, J = 9.7 Hz, 1H, H-7B), 3.71 (dd, J = 9.3, 5.2 Hz, 1H, H-7A), 2.94 (dtd, J = 10.7, 5.6, 1.9 Hz, 1H, H-5). ^{13}C NMR (101 MHz, $CDCl_3$) δ 137.9, 137.5, 137.4, 137.0 (4x C_{qAr}), 128.7, 128.7, 128.6, 128.6, 128.6, 128.4, 128.2, 128.1, 128.0, 127.9, 127.8, 127.7 (CH_{Ar}), 84.6 (C-1), 84.0 (C-6), 77.5 (C-3), 76.3 (C-2), 74.7 (C-4), 74.1, 73.4, 72.8, 72.5 (4x CH_2Ph), 65.0 (C-7), 41.1 (C-5). HRMS: calculated for $[C_{35}H_{36}O_8SNa]^+$ 639.20231, found 639.202340.

(3*aR*,4*S*,5*S*,6*R*,7*R*,7*aR*)-4,5,6-Trihydroxy-7-(hydroxymethyl)hexahydrobenzo[*d*][1,3,2] dioxathiole 2,2-dioxide (5): 20% Palladium hydroxide on carbon (13 mg, 0.018 mmol) was added to a solution of **13** (28 mg, 0.045 mmol) in anhydrous MeOH (5 mL) under Argon atmosphere. The mixture stirred under hydrogen atmosphere for 18 h. Then, filtered through a celite plug and the solvent was evaporated under reduced pressure. The crude was purified by silica flash column chromatography (DCM → DCM/MeOH 9:1) to afford **5** (8.78 mg, 75%). After 4 months in the fridge around 40% degradation is observed. ^{1}H NMR (400 MHz, MeOD) δ 5.16 – 5.03 (m, 2H, H-1, H-6), 4.28 (dd, J = 3.1, 2.1 Hz, 1H, H-4), 4.18 – 4.11 (m, 1H, H-2), 4.02 (td, J = 3.3, 0.9 Hz, 1H, H-3), 3.98 (dd, J = 11.3, 7.2 Hz, 1H, H-7A), 3.84 (dd, J = 11.4, 4.8 Hz, 1H, H-7B), 2.63 (dtdd, J = 6.9, 4.8, 2.1, 0.9 Hz, 1H, H-5). ^{13}C NMR (101 MHz, MeOD) δ 85.6 (C-1/C-6), 84.7 (C-1/C-6), 74.1 (C-3), 71.0 (C-4), 68.5 (C-2), 56.9 (C-7), 45.9 (C-5). HRMS: not found.

(1*R*,2*S*,3*R*,4*R*,5*S*,6*R*)-2-Azido-4,5,6-tris(benzyloxy)-3-((benzyloxy)met-hyl)-cyclohexan-1-ol (15) and (1*R*,2*S*,3*R*,4*R*,5*S*,6*R*)-2-azido-4,5,6-tris(benzyloxy)-3-((benzyloxy)methyl)-cyclohexan-1-ol (16): Fully benzylated β-mannose-configured cyclophellitol **7** (637 mg, 1.19 mmol) was dissolved in anhydrous DMF (30 mL). $LiClO_4$ (1.66 g, 15.6 mmol, 13.0 eq) and NaN_3 (1.01 g, 15.6 mmol, 13.0 eq) were added and the reaction was stirred under N_2 atmosphere overnight at 100 °C. The reaction mixture as cooled to rt and quenched with H_2O. The product was extracted with EtOAc (3x), washed with brine (2x) dried over MgSO4 and concentrated *in vacuo*. Purification by silica column chromatography (pentane /EtOAc 75:25 → 65:35) yielded a 1:1 mixture of two diastereomers: **15** (0.40 g, 0.69 mmol, 58%) and 1-hydroxy-6-azido **16** (93.5 mg, 0.161 mmol, 14%).

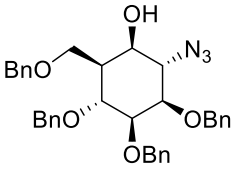

Azide (15): $[\alpha]_D^{20}$ = -19.4 (*c* = 1, $CHCl_3$). IR (neat, cm^{-1}) 3390, 2869, 2109, 1497, 1454, 1265, 1066, 1027, 912, 733, 695. ^{1}H NMR (400 MHz, $CDCl_3$) *δ* 7.39 – 7.14 (m, 20H, CH Ar), 4.71 – 4.39 (m, 8H, $4CH_2Ph$), 3.90 (dt, *J* = 14.6, 8.7 Hz, 3H, H7a), 3.75 (t, *J* = 4.7 Hz, 1H), 3.72 (t, *J* = 3.9 Hz, 1H), 3.67 (dd, *J* = 8.1, 2.9 Hz, 1H), 3.62 (dd, *J* = 9.5, 5.5 Hz, 1H, H-7b), 3.45 (s, 1H, OH), 2.57 (t, *J* = 6.0 Hz, 1H, H-5).^{13}C NMR (101 MHz, $CDCl_3$) *δ* 138.1, 138.0, 137.8 ($4C_q$ Ar), 128.6 - 127.8 (20CH Ar), 78.7 (CH), 75.1 (CH), 73.4, 73.3, 73.2 ($4CH_2Ph$), 70.7 (CH), 68.1 (C-7), 42.8 (C-5) HRMS: Calcd. for $[C_{35}H_{37}N_3O_5 \cdot NH_4]^+$ m/z 597.30730; found m/z 597.30715. HRMS: Calcd. for $[C_{35}H_{37}N_3O_5 \cdot Na]^+$ m/z 602.26225; found m/z 602.26254.

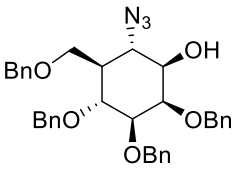

Azide (16): $[\alpha]_D^{20}$ = -35.6 (*c* = 1, $CHCl_3$). IR (neat, cm^{-1}) 2868, 2106, 1454, 1264, 1089, 1027, 731, 697. ^{1}H NMR (400 MHz, $CDCl_3$) *δ* 7.42 – 7.15 (m, 20H, CH Ar), 5.16 (d, *J* = 11.7 Hz, 1H, CH*H*Ph), 4.90 (d, *J* = 10.7 Hz, 1H, CH*H*Ph), 4.75 (dd, 2H, CH_2Ph), 4.67 (d, *J* = 11.7, 1.5 Hz, 1H, CH*H*Ph), 4.56 – 4.49 (m, 2H, CH_2Ph), 4.46 (d, *J* = 12.1 Hz, 1H, CH*H*Ph), 4.10 (t, *J* = 10.3 Hz, 1H), 4.06 (t, *J* = 2.6 Hz, 1H), 3.88 – 3.76 (m, 2H, H-7a), 3.63 (dd, *J* = 9.2, 2.3 Hz, 1H, H-7b), 3.47 – 3.37 (m, 2H), 1.34 (td, *J* = 11.2, 2.0 Hz, 1H, H-5). ^{13}C NMR (101 MHz, $CDCl_3$) *δ* 138.6, 138.6, 138.5, 138.3 ($4C_q$ Ar), 128.7 - 127.7 (20CH Ar), 84.2 (CH), 77.8 (CH), 75.8 (CH), 75.7, 74.8 ($2CH_2Ph$), 74.2 (CH), 73.2, 73.2 ($2CH_2Ph$), 65.1 (C-7), 62.4 (CH), 45.0 (C-5). HRMS: Calcd. for $[C_{35}H_{37}N_3O_5 \cdot NH_4]^+$ m/z 597.30750; found m/z 597.30715. HRMS: Calcd. for $[C_{35}H_{37}N_3O_5 \cdot Na]^+$ m/z 602.26225; found m/z 602.26286.

(1*R*,2*S*,3*R*,4*S*,5*R*,6*S*)-2-Amino-3,4,5-tris(benzyloxy)-6-((benzyloxy)met-hyl)-cyclohexan-1-ol (17): Azide **15** (400 mg, 0.69 mmol, 58%) was dissolved in anhydrous THF (45 mL) and purged with N_2 for 10 minutes. PtO_2 (47 mg, 0.21 mmol, 0.3 eq) was added and the mixture was bubbled with N_2 for another 10 minutes. Subsequently, the reaction was stirred under H_2 atmosphere overnight at rt. After complete conversion, the catalyst was removed by filtration over Celite and the filtrate was concentrated *in vacuo*. Purification by silica column chromatography (pentane /EtOAc 75:25 → 65:35) yielded amine **17** (0.33 g, 0.60 mmol, 86%).

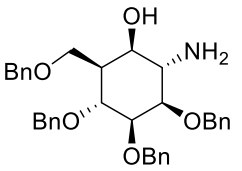

$[\alpha]_D^{20}$ = 2.9 (*c* = 1, $CHCl_3$). IR (neat, cm^{-1}) 2923, 2866, 1497, 1454, 1066, 1027, 733, 695. ^{1}H NMR (400 MHz, $CDCl_3$) *δ* 7.35 – 7.13 (m, 20H, CH Ar), 4.59 – 4.36 (m, 8H), 3.98 – 3.85 (m, 3H, H-7a), 3.76 (t, *J* = 3.6 Hz, 1H), 3.66 (t, 1H, H-7b), 3.59 (dd, *J* = 9.4, 3.0 Hz, 1H), 3.32 – 3.11 (m, 3H), 2.70 – 2.60 (m, 1H, CH-5). ^{13}C NMR (101 MHz, $CDCl_3$) *δ* 138.3, 138.3, 138.1 ($4C_q$ Ar), 128.5 - 127.7 (20CH Ar), 80.2 (CH), 75.3 (CH), 74.8 (CH), 73.2, 72.7, 72.3, 71.3 ($4CH_2Ph$), 71.3 (CH), 68.2 (C-7), 52.9 (CH), 42.6 (C-5). HRMS: Calcd. for $[C_{35}H_{39}NO_5 \cdot H]^+$ m/z 554.28999; found m/z 554.29010.

Benzyl ((1*S*,2*R*,3*S*,4*R*,5*S*,6*R*)-2,3,4-Tris(benzyloxy)-5-((benzyloxy)met-hyl)-6-hydroxycyclohexyl)carbamate (18): Amine **17** (0.15 g, 0.27 mmol) was dissolved in a solution of dioxane and water (1.5:1). K_2CO_3 (12 mg, 85 µmol, 1 eq) was added and the mixture was stirred for 10 minutes. Benzyl chloroformate (15 µL, 0.18 mmol, 1.2 eq) was added and the reaction was vigorously stirred for 1 h. After complete conversion the mixture was diluted with DCM, washed with water (1x) and brine (1x), dried over $MgSO_4$ and concentrated *in vacuo*. Purification by silica column chromatography (pentane /EtOAc 80:20 → 65:35) yielded Cbz-protected amine **18** (150 mg, 0.2 mmol, 74%).

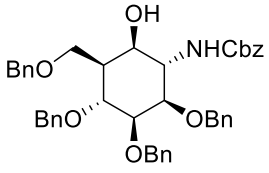

$[\alpha]_D^{20}$ = +8.67 (*c* = 0.3, $CHCl_3$). IR (neat, cm^{-1}): 2865, 1709, 1454, 1093, 736, 697. ^{1}H NMR (400 MHz, $CDCl_3$) *δ* 7.40 –

7.16 (m, 25H, CH Ar), 5.14 – 5.05 (m, 2H, CH_2PhCbz), 4.64 (d, *J* = 11.3 Hz, 3H), 4.58 – 4.47 (m, 5H), 4.42 (d, *J* = 11.9 Hz, 1H), 4.17 (dd, *J* = 6.7 Hz, 1H), 4.01 (dd, *J* = 11.0, 5.2 Hz, 1H), 3.96 – 3.81 (m, 2H, CH-7a), 3.79 – 3.73 (m, 1H, CH-7b), 3.70 (dd, *J* = 6.6, 2.9 Hz, 1H), 2.28 (m, 1H). ^{13}C NMR (101 MHz, $CDCl_3$) *δ* 138.4, 138.3, 138.2, 137.7, 136.4 (5C_q Ar), 128.7 - 127.7 (25CH Ar), 78.2 (CH), 77.6 (CH), 74.8 (CH), 73.4, 73.0, 72.7 (4CH_2Ph), 70.6 (CH), 67.6 (C-7), 67.2 (CH_2PhCbz), 52.7 (CH), 44.1 (C-5). HRMS: Calcd. for $[C_{43}H_{45}NO_7 \cdot H]^+$ m/z 688.32671; found m/z 688.32688.

Benzyl (3a*R*,4*R*,5*S*,6*R*,7*R*,7a*R*) -4,5,6-tris(benzyloxy)-7-((benzyloxy)-methyl) - hexahydro-3*H*-benzo[*d*][1,2,3]oxathiazole-3-carboxylate 2,2-dioxide (19): Cbz-protected amine **11** (0.15 g, 0.17 mmol) was dissolved in dry DCM (3 mL). Imidazole (64 mg, 0.94 mmol, 5.5 eq) and Et_3N (249 µL, 1.79 mmol, 10.5 eq) were added at 0 °C. $SOCl_2$ (123 µL, 0.202 g, 1.70 mmol) was added after 5 minutes at neutral pH. After 1 h the mixture was diluted in cold Et_2O, washed with brine (1x), dried over $MgSO_4$ and concentrated under high vacuum for 1 h. The crude material was dissolved in EtOAc (2.5 mL), CAN (2.5 mL) and H_2O (2.5 ml) and the mixture was cooled to 0 °C. $NaIO_4$ (91 mg, 0.43 mmol, 2.5 eq) was added and subsequently $RuCl_3$ (8.8 mg, 43 µmol, 0.25 eq) and the mixture was stirred for 3 h. The mixture was diluted with EtOAc, washed with sat. aq. $Na_2S_2O_3$, H_2O and brine, dried over $MgSO_4$ and concentrated *in vacuo.* Purification by silica column chromatography (pentane /EtOAc 88:12 → 92:8) yielded the protected cyclosulfamidate **18** (59 mg, 78 µmol, 46%). ^{1}H NMR (400 MHz, $CDCl_3$) *δ* 7.44 – 7.04 (m, 25H), 5.34 (d, *J* = 12.1 Hz, 1H, CH*H*PhCbz), 5.20 (d, *J* = 12.1 Hz, 1H, CH*H*PhCbz), 4.85 (dd, *J* = 11.5, 5.2 Hz, 1H), 4.79 – 4.71 (m, 1H), 4.61 (d, *J* = 12.1 Hz, 1H, CH*H*Ph), 4.49 (d, *J* = 15.9 Hz, 1H, CH*H*Ph), 4.44 (d, 1H, CH*H*Ph), 4.40 (dd, *J* = 7.0, 5.0 Hz, 3H, 3x CH*H*Ph), 4.29 (t, *J* = 12.0 Hz, 2H, CH_2Ph), 4.07 (t, *J* = 2.5 Hz, 1H), 3.86 (t, *J* = 9.6 Hz, 1H, H-7a), 3.81 – 3.77 (m, 2H), 3.67 (dd, *J* = 9.2, 4.9 Hz, 1H, H-7b), 2.90 (dtd, *J* = 10.1, 5.1, 1.9 Hz, 1H, H-5). ^{13}C NMR (101 MHz, $CDCl_3$) *δ* 151.9 (C=O Cbz), 138.0, 137.8, 137.7, 137.3, 134.6 (5Cq Ar), 128.7 - 127.7 (25CH Ar), 79.5 (CH), 78.4 (CH), 76.4 (CH), 74.5 (CH), 73.7, 73.4, 72.5, 72.4 (4CH_2Ph), 69.9 (CH_2PhCbz), 65.2 (C-7), 59.4 (CH), 40.9 (C-5). HRMS: calculated for $[C_{43}H_{44}NO_9S]^+$ 750.27368, found 750.27379.

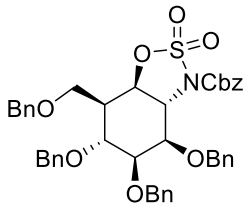

(3a*R*,4*R*,5*S*,6*R*,7*R*,7a*R*)-4,5,6-Trihydroxy-7-(hydroxymethyl)hexahydro-3*H*-benzo[*d*][1,2,3]oxathiazole 2,2-dioxide (6): The protected cyclosulfamidate **19** (27 mg, 36 µmol) was dissolved in MeOH (7.8 mL) and purged with N_2. Pd/C (10 wt%, 34 mg, 31 µmol, 0.4 eq) was added and the mixture was again purged with N_2. Subsequently, the mixture was put under H_2 atmosphere and stirred overnight at rt. The reaction mixture was filtered over a celite plug and concentrated *in vacuo.* Purification by silica column chromatography (DCM /MeOH 95:5 → 85:15) yielded cyclosulfamidate **6** (5.1 mg, 20 µmol, 75%). ^{1}H NMR (400 MHz, MeOD) *δ* 4.76 (dd, *J* = 10.6, 5.8 Hz, 1H, H-6), 4.30 (t, *J* = 2.5 Hz, 1H, H-3), 4.05 (d, *J* = 9.7 Hz, 1H, H-4), 4.01 (d, *J* = 3.5 Hz, 1H, H-7a), 4.00 – 3.96 (m, 1H, H-1), 3.96 – 3.94 (m, 1H, H-2), 3.83 (dd, *J* = 11.2, 4.5 Hz, 1H, H-7b), 2.50 (qd, *J* = 6.9, 5.9, 1.9 Hz, 1H, CH-5). ^{13}C NMR (101 MHz, MeOD) *δ* 86.6 (C-6), 74.8 (C-2), 72.4 (C-3), 70.4 (C-1), 60.6 (C-4), 58.5 (C-7), 46.8 (C-5)

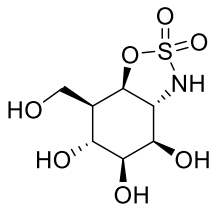

3.6 References

(1) Koshland, D. E. Stereochemistry and the Mechanism of Enzymatic Reactions. *Biol. Rev.* **1953**, *28* (4), 416–436.

(2) Artola, M.; Wu, L.; Ferraz, M. J.; Kuo, C. L.; Raich, L.; Breen, I. Z.; Offen, W. A.; Codée, J. D. C.; van der Marel, G. A.; Rovira, C.; et al. 1,6-Cyclophellitol Cyclosulfates: A New Class of Irreversible Glycosidase Inhibitor. *ACS Cent. Sci.* **2017**, *3* (7), 784–793.

(3) Speciale, G.; Thompson, A. J.; Davies, G. J.; Williams, S. J. Dissecting Conformational Contributions to Glycosidase Catalysis and Inhibition. *Curr. Opin. Struct. Biol.* **2014**, *28* (1), 1–13.

(4) Gloster, T. M.; Davies, G. J. Glycosidase Inhibition: Assessing Mimicry of the Transition State. *Org. Biomol. Chem.* **2010**, *8* (2), 305–320.

(5) Rempel, B. P.; Withers, S. G. Covalent Inhibitors of Glycosidases and Their Applications in Biochemistry and Biology. *Glycobiology* **2008**, *18* (8), 570–586.

(6) Williams, S. J.; Withers, S. G. Glycosyl Fluorides in Enzymatic Reactions. *Carbohydr. Res.* **2000**, *327* (1), 27–46.

(7) Macauley, M. S.; Vocadlo, D. J. Increasing O-GlcNAc Levels: An Overview of Small-Molecule Inhibitors of O-GlcNAcase. *Biochim. Biophys. Acta - Gen. Subj.* **2010**, *1800* (2), 107–121.

(8) Lombard, V.; Golaconda Ramulu, H.; Drula, E.; Coutinho, P. M.; Henrissat, B. The Carbohydrate-Active Enzymes Database (CAZy) in 2013. *Nucleic Acids Res.* **2014**, *42* (D1), 490–495.

(9) Davies, G. J.; Planas, A.; Rovira, C. Conformational Analyses of the Reaction Coordinate of Glycosidases. *Acc. Chem. Res.* **2012**, *45* (2), 308–316.

(10) Beenakker, T. J. M.; Wander, D. P. A.; Offen, W. A.; Artola, M.; Raich, L.; Ferraz, M. J.; Li, K. Y.; Houben, J. H. P. M.; van Rijssel, E. R.; Hansen, T.; et al. Carba-Cyclophellitols Are Neutral Retaining-Glucosidase Inhibitors. *J. Am. Chem. Soc.* **2017**, *139* (19), 6534–6537.

(11) Wu, L.; Armstrong, Z.; Schröder, S. P.; de Boer, C.; Artola, M.; Aerts, J. M.; Overkleeft, H. S.; Davies, G. J. An Overview of Activity-Based Probes for Glycosidases. *Curr. Opin. Chem. Biol.* **2019**, *53*, 25–36.

(12) Withers, S. G.; Rupitz, K.; Street, I. P. 2-Deoxy-2-Fluoro-D-Glycosyl Fluorides. *J. Biol. Chem.* **1988**, *263* (17), 17–20.

(13) Zechel, D. L.; Withers, S. G. Glycosidase Mechanisms: Anatomy of a Finely Tuned Catalyst. *Acc. Chem. Res.* **2000**, *33* (1), 11–18.

(14) Williams, R. J.; Iglesias-Fernández, J.; Stepper, J.; Jackson, A.; Thompson, A. J.; Lowe, E. C.; White, J. M.; Gilbert, H. J.; Rovira, C.; Davies, G. J.; et al. Combined Inhibitor Free-Energy Landscape and Structural Analysis Reports on the Mannosidase Conformational Coordinate. *Angew. Chemie - Int. Ed.* **2014**, *53* (4), 1087–1091.

(15) Males, A.; Raich, L.; Williams, S. J.; Rovira, C.; Davies, G. J. Conformational Analysis of the Mannosidase Inhibitor Kifunensine: A Quantum Mechanical and Structural Approach. *ChemBioChem* **2017**, *18* (15), 1496–1501.

(16) Males, A.; Speciale, G.; Williams, S. J.; Davies, G. J. Distortion of Mannoimidazole Supports a B2,5 Boat Transition State for the Family GH125 α-1,6-Mannosidase from Clostridium Perfringens. *Org. Biomol. Chem.* **2019**, *17* (34), 7863–7869.

(17) Davies, G. J.; Williams, S. J. Carbohydrate-Active Enzymes: Sequences, Shapes, Contortions and Cells. *Biochem. Soc. Trans.* **2016**, *44* (1), 79–87.

(18) Rovira, C.; Males, A.; Davies, G. J.; Williams, S. J. Mannosidase Mechanism: At the Intersection of Conformation and Catalysis. *Curr. Opin. Struct. Biol.* **2020**, *62*, 79–92.

(19) Thompson, A. J.; Dabin, J.; Iglesias-Fernández, J.; Ardèvol, A.; Dinev, Z.; Williams, S. J.; Bande, O.; Siriwardena, A.; Moreland, C.; Hu, T. C.; et al. The Reaction Coordinate of a Bacterial GH47 α-Mannosidase: A Combined Quantum Mechanical and Structural Approach. *Angew. Chemie - Int. Ed.* **2012**, *51* (44), 10997–11001.

(20) Herscovics, A. Structure and Function of Class I A1,2-Mannosidases Involved in Glycoprotein Synthesis and Endoplasmic Reticulum Quality Control. *Biochimie* **2001**, *83* (8), 757–762.

(21) van Rijssel, E.; Janssen, A.; Males, A.; Davies, G.; van der Marel, G.; Overkleeft, H. S.; Codée, J. Conformational Behaviour of Mannuronic Acid Based Azasugars. *ChemBioChem* **2017**, *18* (13), 1297–1304.

(22) Kok, K.; Kuo, C.-L.; Katzy, R. E.; Lelieveld, L. T.; Wu, L.; Roig-Zamboni, V.; van der Marel, G. A.; Codée, J. D. C.; Sulzenbacher, G.; Davies, G. J.; et al. 1,6-Epi-Cyclophellitol Cyclosulfamidate Is a Bona Fide Lysosomal α-Glucosidase Stabilizer for the Treatment of Pompe Disease. *J. Am. Chem. Soc.* **2022**, *144* (32), 14819–14827.

(23) Artola, M.; Hedberg, C.; Rowland, R. J.; Raich, L.; Kytidou, K.; Wu, L.; Schaaf, A.; Ferraz, M. J.; van der Marel, G. A.; Codée, J. D. C.; et al. α-d-Gal-Cyclophellitol Cyclosulfamidate Is a Michaelis Complex Analog That Stabilizes Therapeutic Lysosomal α-Galactosidase A in Fabry Disease. *Chem. Sci.* **2019**, *10* (40), 9233–9243.

(24) Chen, Y.; Armstrong, Z.; Artola, M.; Florea, B. I.; Kuo, C.-L.; de Boer, C.; Rasmussen, M. S.; Abou Hachem, M.; van der Marel, G. A.; Codée, J. D. C.; et al. Activity-Based Protein Profiling of Retaining α-Amylases in Complex Biological Samples. *J. Am. Chem. Soc.* **2021**, *143*, 2423–2432.

(25) Bishop, A. C.; Shah, K.; Liu, Y.; Witucki, L.; Kung, C.; Shokat, K. M. Design of Allele-Specific Inhibitors to Probe Protein Kinase Signaling. *Curr. Biol.* **1998**, *8* (5), 257–266.

(26) Shah, K.; Liu, Y.; Deirmengian, C.; Shokat, K. M. Engineering Unnatural Nucleotide Specificity for Rous Sarcoma Virus Tyrosine Kinase to Uniquely Label Its Direct Substrates. *Proc. Natl. Acad. Sci.* **1997**, *94* (8), 3565–3570.

(27) Schumann, B.; Malaker, S. A.; Wisnovsky, S. P.; Debets, M. F.; Agbay, A. J.; Fernandez, D.; Wagner, L. J. S.; Lin, L.; Li, Z.; Choi, J.; et al. Bump-and-Hole Engineering Identifies Specific Substrates of Glycosyltransferases in Living Cells. *Mol. Cell*

3.7 Appendix

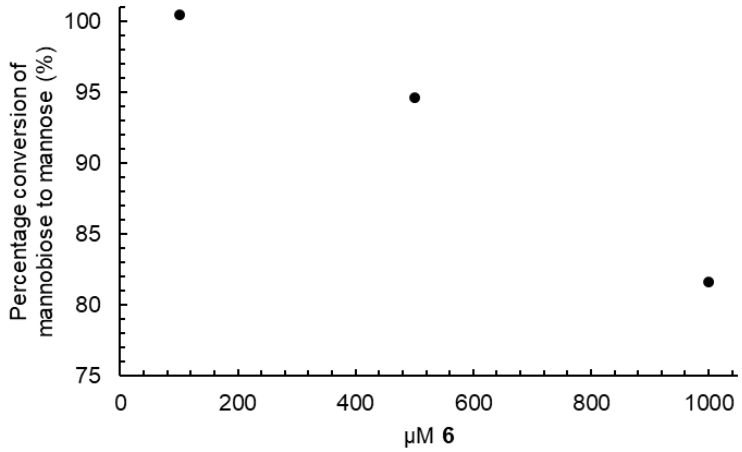

Figure S3.1. Inhibition of *Ck*GH47 by **6** monitored by the enzymatic conversion of mannobiose to mannose. Three concentrations of the inhibitor were incubated with 200 nM of *Ck*GH47 for 45 minutes at 22 °C, subsequently, 189 μM of α-1,2-mannobiose was added and the reaction was incubated for 1 hour at 22 °C. The enzyme was heat denatured (90 °C for 5 minutes). Using the mannose detection kit, NADPH production at 340 nm was measured and converted to mannose concentration using a standard curve of mannose.

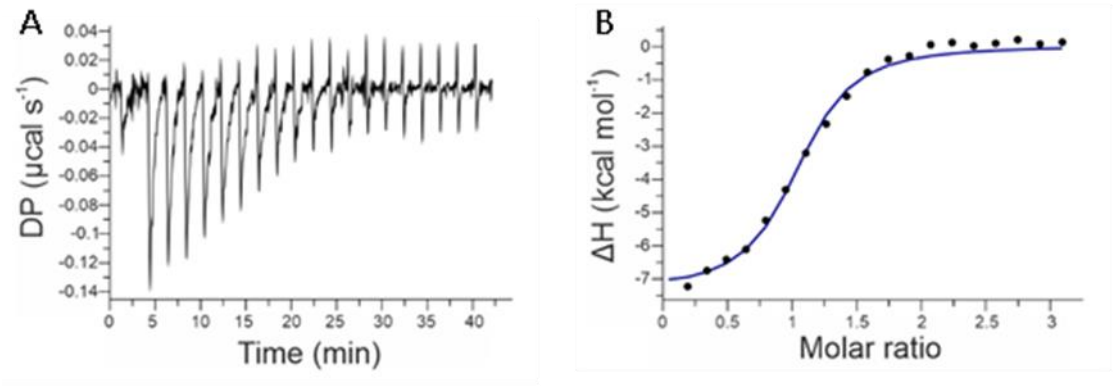

Figure S3.2. Isothermal titration calorimetry binding thermodynamics between *Ck*GH47 L310S and **6**. A. raw data injection profile; B. Titration curve. N = 1.01 ± 0.02 sites, ΔH = -7.39 ± 0.19 kcal mol^{-1}.

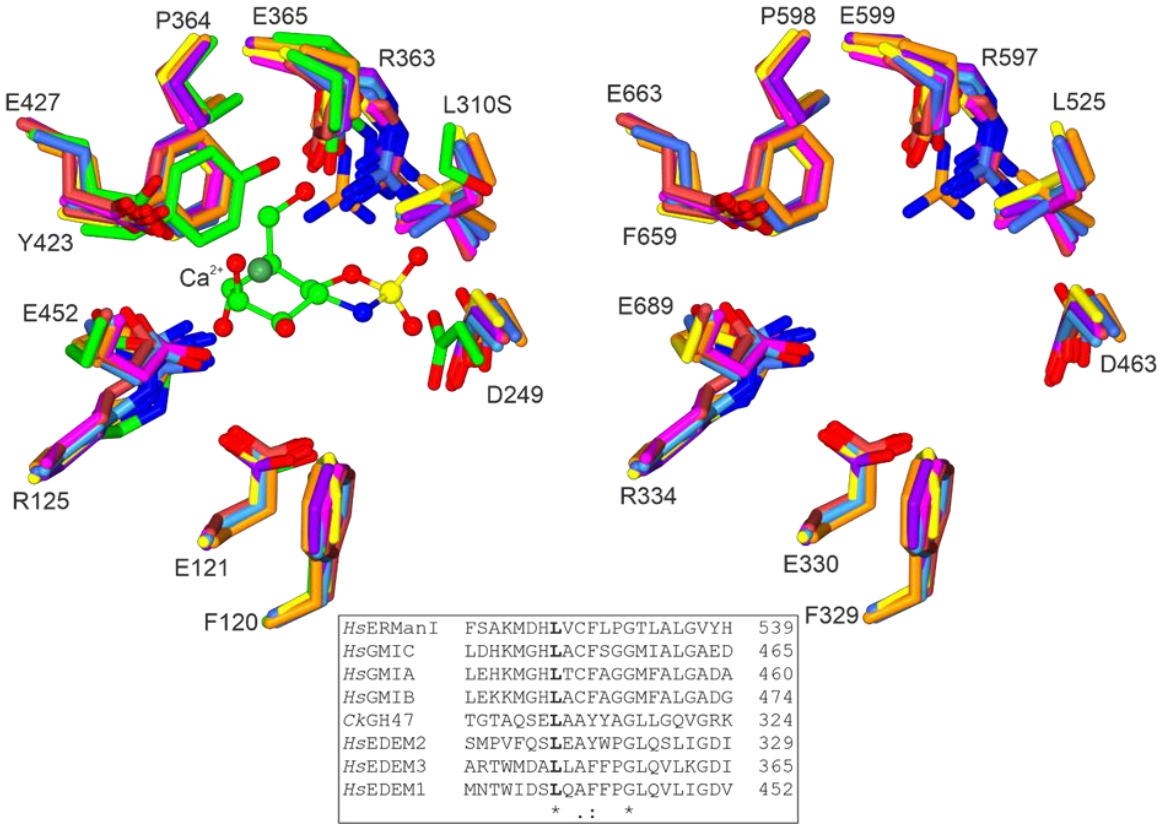

Figure S3.3. Overlay of the human GH47 α-1,2-mannosidase structures highlighting the conserved active site. Crystal structure of ERManI is in orange (PDB ID: 1FMI); the remaining structures were predicted by Alphafold[5], in light blue is GMIB, in dark blue is GMIA, in purple is GMIC, in yellow is EDEM2, in red is EDEM3 and in pink is EDEM1. The crystal structure from this work of *Ck*GH47 and **3** is in green. Residues annotated according to the numbering of *Ck*GH47. The figure on the right lacks the *Ck*GH47 enzyme and the residues are annotated according to the numbering of *Hs*ERManI.

Table S3.1. Catalytic activity of WT and L310S *Caulobacter* GH47 mannosidase.

	***Ck*GH47 WT**	***Ck*GH47 L310S**
V_{max} (μM s^{-1})	1.29 ± 0.09	0.154 ± 0.01
K_M (μM)	65.7 ± 14.2	402.8 ± 71.3
k_{cat} (s^{-1})	6.45	0.308
k_{cat}/K_M (μM^{-1} s^{-1})	0.098	0.0076
K_i α-1,2-mannobiose (mM)		42.7 ± 24.8
K_i **3** (nM)	n.d.	574
K_D **3** (nM)	n.d.	970±158

Table S3.2. Data statistics for data collection and structural refinement of *Ck*GH47 in complex with **6**.

	*Ck*GH47
Ligand	**6**
PDB code	**8B5M**
Data collection	
Wavelength (Å)	0.799
Space group	*H*3
Cell dimensions:	
a, *b*, *c* (Å)	144.13, 144.13, 50.32
α, β, γ (°)	90, 90, 120
Resolution (Å)	72.02-0.97 (0.99-0.97)
R_{merge}	0.16 (1.49)
R_{pim}	0.05 (0.49)
CC (1/2)	1.00 (0.61)
$I / \sigma I$	7.7 (1.3)
Completeness (%)	100.0 (100.0)
Redundancy	10.2 (10.0)
Refinement	
Resolution (Å)	72.02-0.97 (0.99-0.97)
No. reflections	230864
R_{work} / R_{free}	0.14/0.15
No. atoms	
Protein	3554
Ligands/Ions	16/3
Water	715
B-factors (Å^2)	
Protein	7
Ligand/Ions	5/4
Water	19
R.m.s. deviations	
Bond lengths (Å)	0.014
Bond angles (°)	1.9
Ramachandran	
Favoured (%)	96.5
Allowed (%)	3.0
Outliers (%)	0.5